PCP
PLANT & CELL PHYSIOLOGY

The Mode of Action of Endosidin20 Differs from That of Other Cellulose Biosynthesis Inhibitors

Lei Huang [1,2] and Chunhua Zhang [1,2,*]

[1]Department of Botany and Plant Pathology, Purdue University, 915 W. State Street, West Lafayette, IN 47907, USA
[2]Purdue Center for Plant Biology, Purdue University, 610 Purdue Mall, West Lafayette, IN 47907, USA
*Corresponding author: E-mail, zhang150@purdue.edu; Fax, +1-765-494-0363.
(Received 8 July 2020; Accepted 11 October 2020)

Endosidin20 (ES20) was recently identified as a cellulose biosynthesis inhibitor (CBI) that targets the catalytic domain of CELLULOSE SYNTHASE 6 (CESA6) and thus inhibits the growth of *Arabidopsis thaliana*. Here, we characterized the effects of ES20 on the growth of other plant species and found that ES20 is a broad-spectrum plant growth inhibitor. We tested the inhibitory effects of previously characterized CBIs (isoxaben, indaziflam and C17) on the growth of Arabidopsis *cesa6* mutants that have reduced sensitivity to ES20. We found that most of these mutants are sensitive to isoxaben, indaziflam and C17, indicating that these tested CBIs have a different mode of action than ES20. ES20 also has a synergistic inhibitory effect on plant growth when jointly applied with other CBIs, further confirming that ES20 has a different mode of action than isoxaben, indaziflam and C17. We demonstrated that plants carrying two missense mutations conferring resistance to ES20 and isoxaben can tolerate the dual inhibitory effects of these CBIs when combined. ES20 inhibits Arabidopsis growth in growth medium and in soil following direct spraying. Therefore, our results pave the way for using ES20 as a broad-spectrum herbicide, and for the use of gene-editing technologies to produce ES20-resistant crop plants.

Keywords: Cellulose • Cellulose biosynthesis Inhibitor • Cellulose synthase • Endosidin20 • Herbicide.

Introduction

Cellulose microfibrils are crystalline polymers of β-1,4-D-glucose units that serve as the main load-bearing component of plant cell walls. Cellulose is biosynthesized by the rosette-structured cellulose synthase (CESA) complex (CSC) at the plasma membrane (PM) (Mueller et al. 1976, Giddings et al. 1980, Mueller and Brown 1980). Each CSC consists of 18 CESAs of three different isoforms in a 1:1:1 molar ratio (Doblin et al. 2002, Fernandes et al. 2011, Newman et al. 2013, Gonneau et al. 2014, Hill et al. 2014, Oehme et al. 2015, Wang et al. 2015, Nixon et al. 2016, Wang and Hong 2016, Jarvis 2018, Kubicki et al. 2018, Turner and Kumar 2018, Purushotham et al. 2020). Arabidopsis CSCs that biosynthesize the primary cell wall are composed of CESA1, CESA3 and CESA6 or a CESA6-like subunit (CESA2, CESA5 or CESA9), whereas the CSCs that biosynthesize the secondary cell wall are composed of CESA4, CESA7 and CESA8 (Taylor et al. 2003, Desprez et al. 2007, Persson et al. 2007).

Electron micrographs of freeze-fractured plant cells revealed that the rosette-structured CSCs are located at the PM, Golgi and post-Golgi vesicles (Haigler and Brown 1986). More recent live-cell imaging using functional fluorescence-tagged CESAs confirmed that CSCs are localized at the PM, Golgi, trans-Golgi network and vesicles called microtubule-associated CESA compartments or small CESA compartments (Paredez et al. 2006, Crowell et al. 2009, Gutierrez et al. 2009). CSCs at the PM undergo bidirectional movement using microtubules as a guide, powered by cellulose polymerization (Paredez et al. 2006, Fujita et al. 2013).

CSC subcellular transport requires the vesicle trafficking machinery and other CESA-interacting proteins. STELLO interacts with multiple CESAs to control the efficient exit of the CSCs from the Golgi (Zhang et al. 2016). POM2/CELLULOSE SYNTHASE INTERACTIVE PROTEIN 1 directly interacts with CESAs in the central cytoplasmic domain to associate the CSCs with microtubules (Gu et al. 2010, Bringmann et al. 2012, Lei et al. 2012). Moreover, COMPANION OF CELLULOSE SYNTHASE 1 interacts with CESAs to regulate CSC transport under salt stress (Endler et al. 2015). Successful CSC delivery to the PM also requires the coordinated functions of ACTIN, MYOSIN XI, the exocyst complex and PATROL1 (Sampathkumar et al. 2013, ZHu et al. 2018, Zhang et al. 2019). The newly identified SHOU4 protein negatively regulates CSC delivery to the PM, while clathrin-mediated endocytosis removes CSCs from the PM (Bashline et al. 2013, Polko et al. 2018). Therefore, cellulose biosynthesis is a complex process involving the coordinated function of multiple proteins.

Cellulose biosynthesis inhibitors (CBIs) are small molecules that inhibit cellulose biosynthesis by targeting CESAs or other proteins required for cellulose biosynthesis. CBIs often inhibit plant growth, cause cell swelling and/or affect CSC subcellular localization (Debolt et al. 2007, Harris et al. 2012, Brabham et al. 2014, Xia et al. 2014, Worden et al. 2015, Hu et al. 2016,

Plant Cell Physiol. 61(12): 2139–2152 (2020) doi:10.1093/pcp/pcaa136, Advance Access publication on 26 October 2020, available online at https://academic.oup.com/pcp

Tateno et al. 2016). Isoxaben is a well-characterized CBI that has been widely used to study the mechanisms of cellulose biosynthesis. Isoxaben was originally used as an herbicide to control broad-leaf weeds because of its high-efficiency inhibition of plant growth (Huggenberger and Gueguen 1987, Jamet and Thoisy-Dur 1988, Brinkmeyer et al. 1989), which was later found to be caused by its alteration of plant cell wall composition (Heim et al. 1990). Single amino acid mutations in CESA3 and CESA6 promoted the plant tolerance of isoxaben (Scheible et al. 2001, Desprez et al. 2002), providing evidence that this CBI inhibits plant growth by targeting CESAs. Live-cell imaging of isoxaben-treated plants expressing fluorescence-tagged CESAs revealed that this herbicide rapidly depletes the CSCs from the PM (Paredez et al. 2006), which makes it useful for the elucidation of CSC subcellular trafficking.

A recently characterized small molecule, C17, also depletes CSCs from the PM and inhibits plant cytokinesis, root growth and cellulose biosynthesis (Hu et al. 2016). Mutations in *CESA1*, *CESA3* and the genes encoding some pentatricopeptide repeat-like proteins can overcome the inhibitory effect of C17 on plant growth (Hu et al. 2016). The inhibitor of mitochondrial complex III can also reduce plant sensitivity to C17 treatment, indicating that C17 might have a complex mode of action instead of directly targeting CESAs to inhibit plant growth. C17 has an inhibitory effect on a variety of plant species and may therefore be a good candidate for broad-spectrum herbicide development (Hu et al. 2019).

Indaziflam is a potent CBI that has been commercialized as an herbicide; it functions by increasing the abundance of the CSCs at the PM, which counterintuitively inhibits cellulose biosynthesis via an unknown mechanism (Brabham et al. 2014). CESTRIN reduces the cellulose content of plant cell walls and removes CSCs from the PM, but its endogenous target protein has not been identified (Worden et al. 2015). Morlin is an inhibitor of microtubule dynamics and, in turn, affects the trajectories of CSC at the PM (Debolt et al. 2007). This collection of CBIs allows the transient manipulation of the cellulose biosynthesis process and provides candidate small molecules for herbicide development.

Endosidin20 (ES20) inhibits cellulose biosynthesis in *Arabidopsis thaliana* by targeting the catalytic site of CESA6 (Huang et al. 2020). Multiple missense mutations in *CESA6* reduce plant sensitivity to ES20, limiting its effect on the growth of these mutants (Huang et al. 2020). Here, we report the characterization of ES20 and its inhibitory effect on different plant species and compare its mode of action with those of isoxaben, indaziflam and C17. Most mutants with reduced sensitivity to ES20 are sensitive to isoxaben, indaziflam and C17. We show that ES20 is a broad-spectrum plant growth inhibitor with a different mode of action than the other CBIs and can act synergistically in combination with these three tested CBIs to further inhibit plant growth. We show that ES20 has the potential to be used as a commercial herbicide and identify a strategy to create plants with a reduced sensitivity to both ES20 and isoxaben using gene editing.

Results

ES20 is a broad-spectrum plant growth inhibitor

The previous characterization of ES20 activity in Arabidopsis showed that it targets the catalytic site of CESA6, which is a highly conserved sequence among the CESAs (Huang et al. 2020). This high level of amino acid conservation at the catalytic site indicates that ES20 might be a broad-spectrum plant growth inhibitor that targets CESAs in different plants. The mutations of CESA1^{D604N} and CESA7^{P557T} also cause reduced sensitivity to ES20, indicating ES20 targets other CESAs in addition to CESA6 (Huang et al. 2020). Sequence comparison of Arabidopsis CESA6 homologs in rice (*Oryza sativa*), tomato (*Solanum lycopersicum*), soybean (*Glycine max*), *Nicotiana benthamiana* and maize (*Zea mays*) indicates that plant CESA6 homologs share very similar protein sequences (**Supplementary Fig. S1**). The Arabidopsis CESA6 amino acids that cause reduced sensitivity to ES20 when mutated are all conserved in these selected species (**Supplementary Fig. S1**). Here, we tested the effects of ES20 on the growth of various dicotyledonous and monocotyledonous plant species by germinating seeds on vertical plates with the growth medium with agar or on filter paper soaked with water containing ES20. We found that ES20 significantly inhibited the root growth of all the plant species we tested. ES20 inhibited the growth of the dicotyledon plants dandelion (*Taraxacum officinale*), *N. benthamiana*, tomato and soybean at a concentration of 5 μM (**Fig. 1A–H**). ES20 inhibited the growth of the monocotyledon rice and maize at a concentration of 20 μM (**Fig. 1I–L**). The inhibition of the growth of two grasses, perennial ryegrass (*Lolium perenne*) and Kentucky bluegrass (*Poa pratensis*), requires a concentration of 50 μM ES20 (**Fig. 1M–P**). Among the plants we tested, dandelion and the previously tested Arabidopsis are common weeds found in agricultural fields and lawns (Meyerowitz 1989, Yu et al. 2019). The inhibitory effects of ES20 on both dicotyledonous and monocotyledonous plants indicate that ES20 is a broad-spectrum plant growth inhibitor.

To test whether ES20 could affect plant growth via a direct application onto the leaf surfaces, we sprayed soil-grown wild-type (Col-0) Arabidopsis plants with ES20 and monitored their phenotypes. We transferred 5-day-old Col-0 seedlings grown on the half-strength Murashige and Skoog ($^1/_2$ MS) medium into the soil, and 2 d later sprayed them with 50 ml sterile water containing DMSO (0.5%) or ES20 (500 μM), respectively. Seven days after spraying, the ES20-treated seedlings had almost completely died, while the DMSO-treated seedlings exhibited normal growth (**Fig. 1Q**). These small-scale experiments indicate that ES20 has the potential to inhibit plant growth when directly sprayed onto the leaf surfaces.

Analysis of the structure–activity relationship of ES20

ES20 (4-methoxy-*N*-{[2-(2-methylbenzoyl)hydrazino]carbothioyl}benzamide) is a carbonothioyl benzamide derivative. To better understand the pharmacophore of ES20 that is

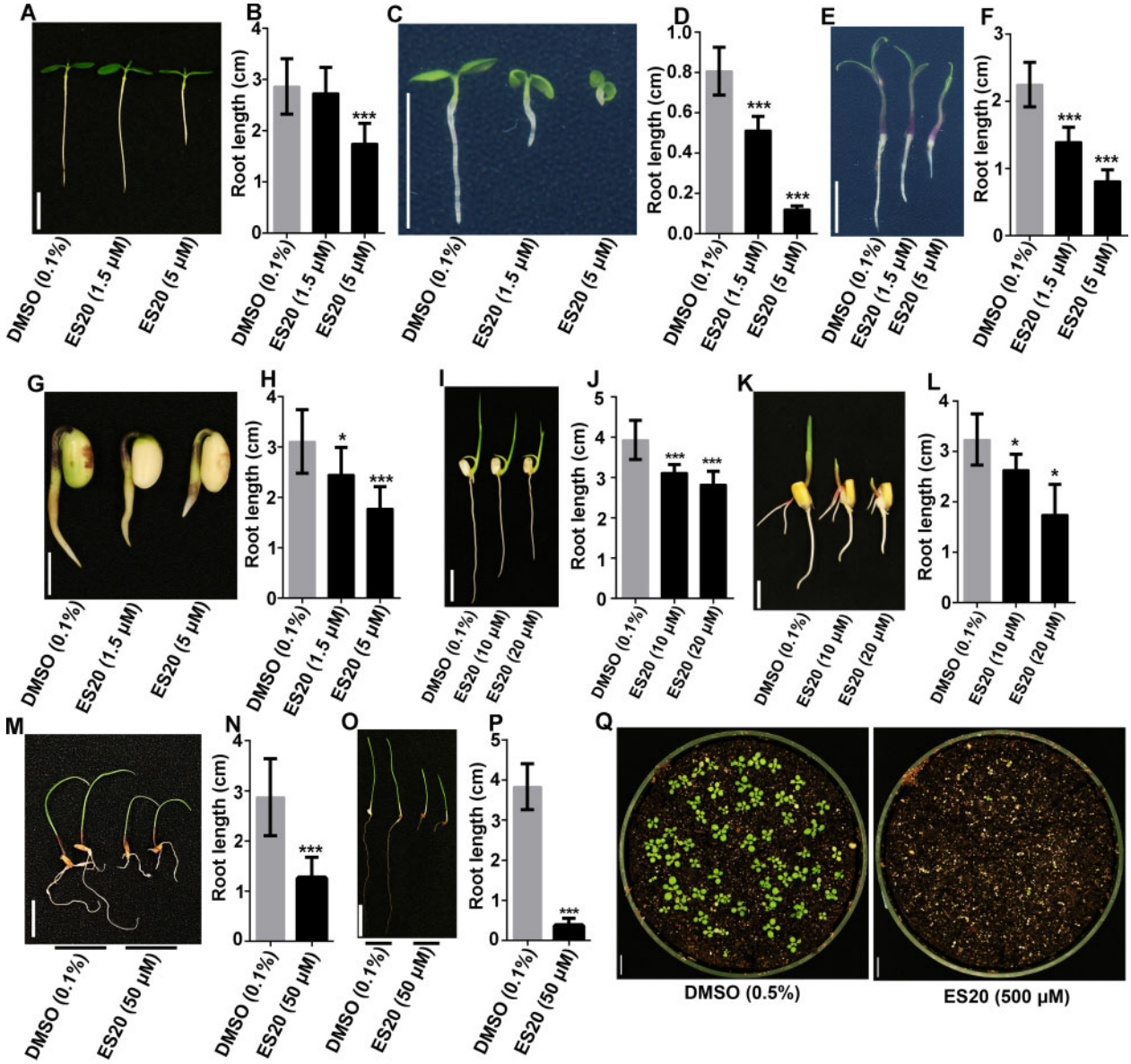

Fig. 1 ES20 is a broad-spectrum plant growth inhibitor. (A–P) ES20 inhibits plant growth when seeds were germinated and grown in the presence of ES20. Representative seedlings of 5-day-old dandelion (A), tobacco (C), tomato (E), soybean (G), rice (I), maize (K), perennial ryegrass (M) and Kentucky bluegrass (O) treated with DMSO (0.1%) and the indicated concentration of ES20 are presented. The perennial ryegrass and Kentucky bluegrass seeds were soaked in sterile water supplemented with the corresponding treatment, whereas the seeds of the other species were grown on solid $\frac{1}{2}$ MS growth medium supplemented with the indicated treatment. (Q) Spraying ES20 inhibits the growth of soil-grown Arabidopsis. Arabidopsis Col-0 was grown on soil sprayed with DMSO (0.5%; left) or ES20 (500 μM; right). Images were taken 7 d after spraying. Scale bars: 1 cm. (B, D, F, H, J, L, N and P) Quantification of the root lengths in (A), (C), (E), (G), (I), (K), (M) and (O), respectively. $^{*}P < 0.05$ and $^{***}P < 0.001$ (two-tailed Student's *t*-test), in comparison with the DMSO control treatment. The data represent the mean ± SD. $N = 10$, 15, 10, 8, 12, 10, 10 and 9 for panels (B), (D), (F), (H), (J), (L), (N) and (P), respectively.

essential for the inhibition of plant growth, we tested 11 ES20 analogs for their effect on plant growth (**Fig. 2A**). We grew Arabidopsis Col-0 seedlings on 1 μM of the different analogs and compared their root lengths with those of the DMSO control (**Fig. 2B, C**). Among the compounds we tested, only ES20 significantly inhibited root growth in Col-0.

After comparing the structures of the 11 analogs with that of ES20, we found that the presence and position of the 4-methoxy group are essential for the inhibitory effect of ES20, as the analogs in which the 4-methoxy group is changed to another group or another location on the compound could not actively inhibit root growth. Similarly, the analogs in which the methylbenzoyl group had been changed or moved to another location could not actively inhibit plant growth. Moreover, the analogs that altered the methylbenzoyl group by replacing the benzyl group or changing the position of the methyl group did not inhibit plant growth. Therefore, the 4-methoxy and methylbenzoyl groups and their locations are key for ES20 function.

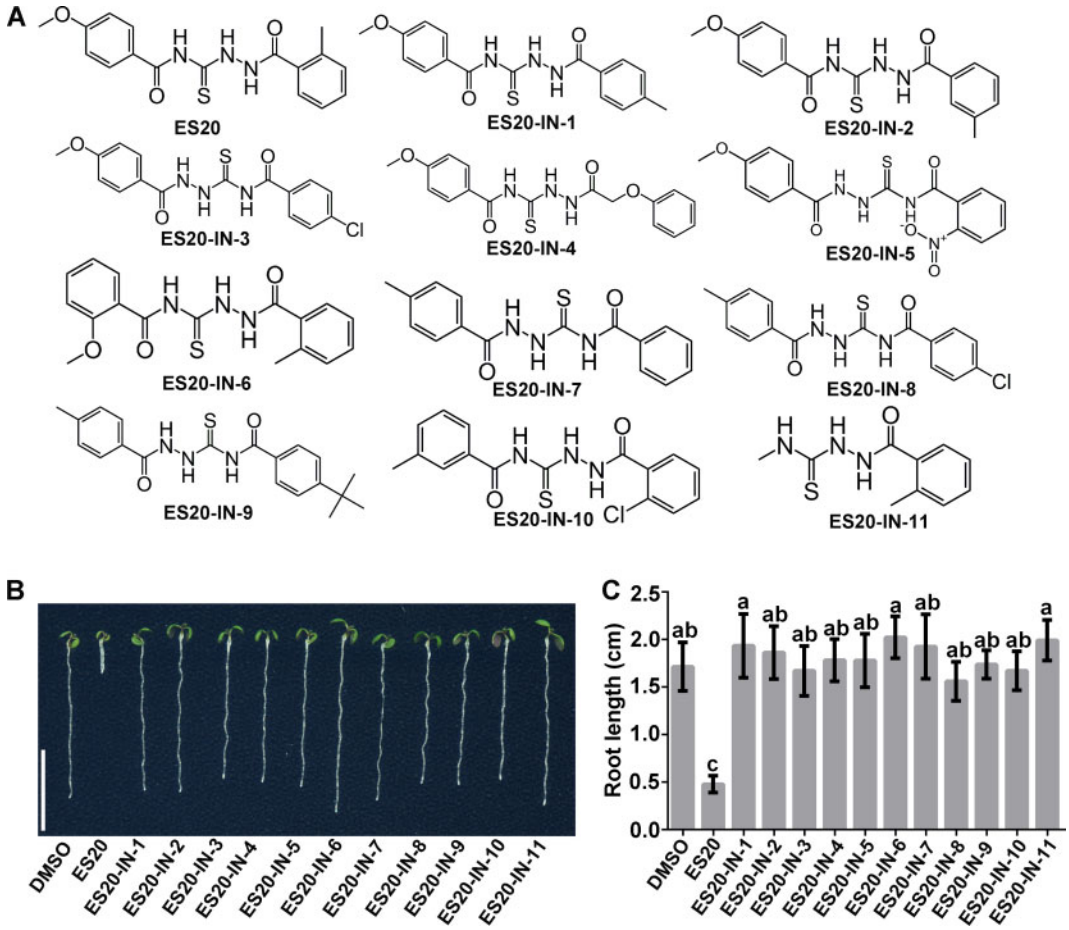

Fig. 2 ES20 structure–activity relationship analysis. (A) Chemical structures of ES20 and 11 analogs. (B) Representative 5-day-old Arabidopsis Col-0 seedlings grown on $^1/_2$ MS growth medium supplemented with DMSO (0.1%) or 1 μM of the indicated analog. Scale bar: 1 cm. (C) Quantification of the root lengths of the seedlings shown in (B). The data represent the mean ± SD. $N = 10$. Different letters indicate a statistically significant difference ($P < 0.05$), as determined using a one-way Analysis of Variance (ANOVA) followed by Tukey's multiple comparison test.

ES20 uses a different mode of action than isoxaben, indaziflam and C17 to inhibit cellulose biosynthesis

The chemical structures of ES20, isoxaben, indaziflam and C17 are quite different (**Supplementary Fig. S2**), indicating that they might use different modes of action to inhibit cellulose biosynthesis. Although genetic data suggest isoxaben targets Arabidopsis CESA3 and CESA6 (Scheible et al. 2001, Desprez et al. 2002), the direct target proteins of indaziflam and C17 are not clear. We compared their activities with that of ES20. All four tested CBIs inhibit Arabidopsis growth with different efficiencies. Indaziflam was the most efficient at inhibiting the growth of the control plants (**Fig. 3**). The roots of 5-day-old Arabidopsis plants grown in the presence of 0.25 nM indaziflam were only about 30% as long as those grown in the DMSO control medium. Isoxaben and C17 inhibited Arabidopsis root growth by >50% at concentrations of 8 and 200 nM, respectively. As reported previously (Huang et al. 2020), ES20 inhibits about 80% of Arabidopsis root growth at a concentration of 1 μM (**Fig. 3**; SYP61-CFP and PIN2-GFP control plants).

Previously, we identified 15 *cesa6* alleles that carry ethyl methanesulfonate (EMS)-induced missense mutations at *CESA6* with reduced sensitivity to ES20 inhibition and named them ES20-resistant (*es20r*) mutants (Huang et al. 2020). We tested whether these mutants that have reduced sensitivity to ES20 also have altered sensitivity to isoxaben, indaziflam or C17. When we grew these ES20-resistant mutants in growth media supplemented with 1 μM ES20, all of them showed a reduced sensitivity to ES20 when compared with the SYP61-CFP and PIN2-GFP control plants that have the same genetic background as these mutants (**Fig. 3**). In the presence of 8 nM isoxaben, 0.25 nM indaziflam or 200 nM C17, the growth of most of the *es20r* mutants was inhibited to a similar level as the control plants; however, some of the *es20r* mutants showed a reduced sensitivity to isoxaben, indaziflam and C17. Based on the quantification of the relative root growth inhibition, *es20r1* ($CESA6^{E929K}$), *es20r3* ($CESA6^{G935E}$), *es20r4* ($CESA6^{D605N}$), *es20r5* ($CESA6^{S360N}$) and *es20r10* ($CESA6^{P595S}$) had reduced sensitivity to isoxaben; *es20r1* ($CESA6^{E929K}$), *es20r3* ($CESA6^{G935E}$), *es20r4* ($CESA6^{D605N}$) and *es20r5* ($CESA6^{S360N}$) had reduced sensitivity to indaziflam; and *es20r3* ($CESA6^{G935E}$), *es20r4* ($CESA6^{D605N}$), *es20r5* ($CESA6^{S360N}$), *es20r6* ($CESA6^{D602N}$), *es20r7* ($CESA6^{S394F}$) and *es20r12* ($CESA6^{G780S}$) had reduced sensitivity to C17. The different sensitivities of the mutants to these CBIs imply that ES20 has a different target site than the other three CBIs. We found that *es20r3* ($CESA6^{G935E}$), *es20r4* ($CESA6^{D605N}$) and *es20r5*

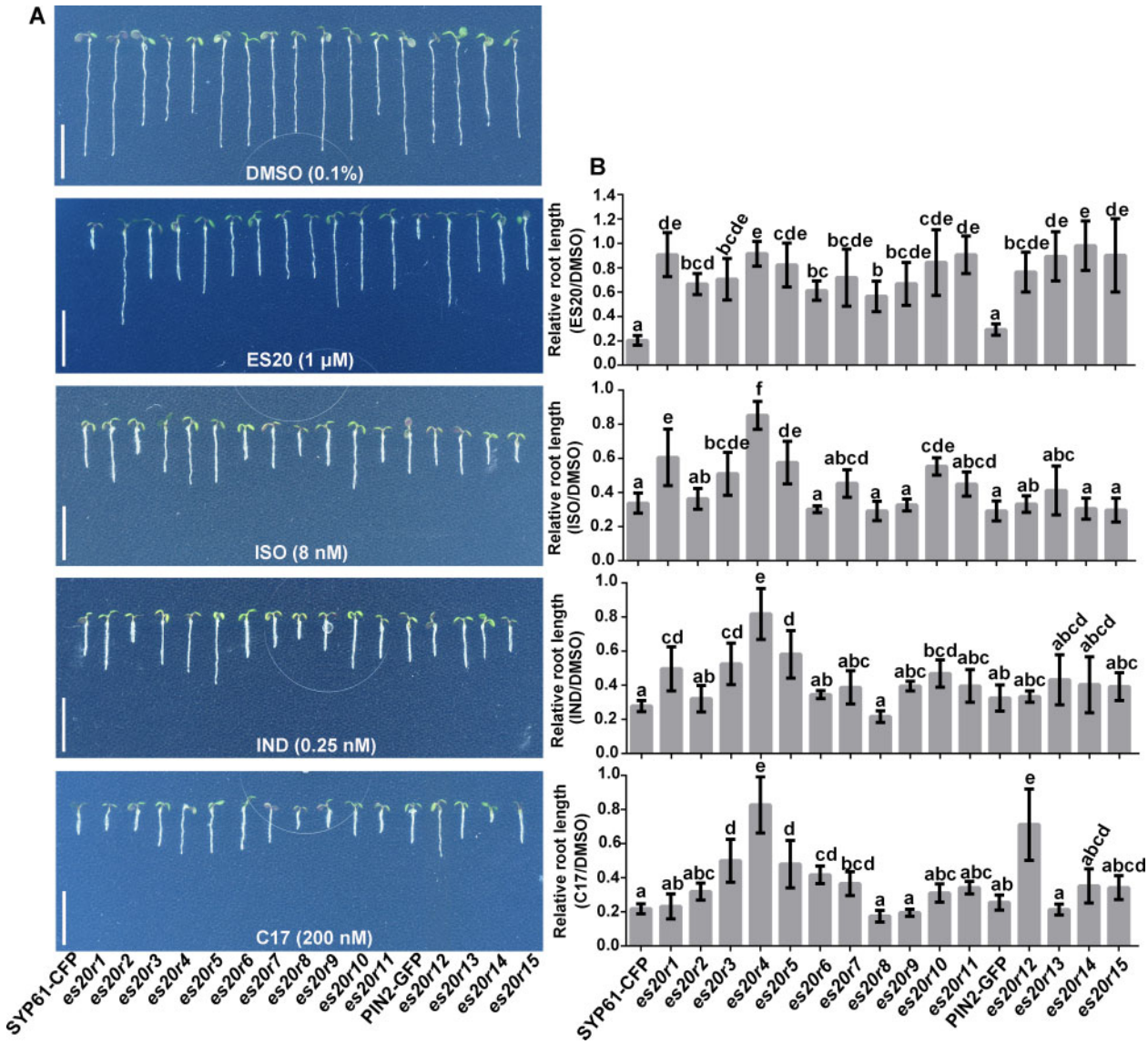

Fig. 3 The growth of the ES20-resistant (*es20r*) mutants in the presence of isoxaben, indaziflam and C17. (A) Representative 5-day-old *es20r*s seedlings grown on $^1/_2$ MS medium supplemented with DMSO (0.1%), ES20 (1 μM), isoxaben (8 nM; ISO), indaziflam (0.25 nM; IND) or C17 (200 nM). Scale bars: 1 cm. (B) Quantification of the relative root lengths of the seedlings shown in (A). Different letters indicate a statistically significant difference ($P < 0.05$), as determined using a one-way ANOVA followed by Tukey's multiple comparison test. The data represent the mean ± SD. $N = 12$.

(CESA6^{S360N}) have reduced sensitivity to all three inhibitors, indicating that these inhibitors may share some common characters in affecting cellulose synthesis.

In our previous study, we found that, in addition to the EMS-induced ES20-resistant mutants, transgenic plants expressing CESA6 carrying predicted mutations at the catalytic site (CESA6^{D562N}, CESA6^{D564N}, CESA6^{D785N}, CESA6^{Q823E}, CESA6^{R826A} and CESA6^{W827A}) in the background of *cesa6* null mutant *procuste 1* (*prc1-1*) have reduced sensitivity to ES20 in terms of growth (Huang et al. 2020). To further explore whether ES20 and the other CBIs have the same binding site, we examined how the six predicted mutations at the catalytic site and two predicted mutations beyond the catalytic site (CESA6^{L365F} and CESA6^{D395N}) in CESA6 affected the responses to the three CBIs. Consistent with the previous results, the six predicted mutations in the catalytic site caused reduced sensitivity to ES20, but the two predicted mutations beyond the catalytic site did not affect the plants' sensitivity to ES20 (**Fig. 4**). By contrast, none of the predicted mutations affected the plant sensitivity to the other three CBIs. These results further imply that ES20 has a different target site than the other three CBIs.

Three mutations, *isoxaben resistance* (*ixr*)*1-1* (CESA3^{G998D}), *ixr1-2* (CESA3^{T942I}) and *ixr2-1* (CESA6^{R1064W}), were previously reported to cause reduced sensitivity to isoxaben (Scheible et al. 2001, Desprez et al. 2002). Isoxaben is thus believed to target these CESAs directly to inhibit cellulose biosynthesis and has been widely used in cellulose biosynthesis research (Scheible et al. 2001, Desprez et al. 2002, Shim et al. 2018). These three mutations are located in the C-terminal regions of the corresponding CESAs, but most of the mutations that cause a

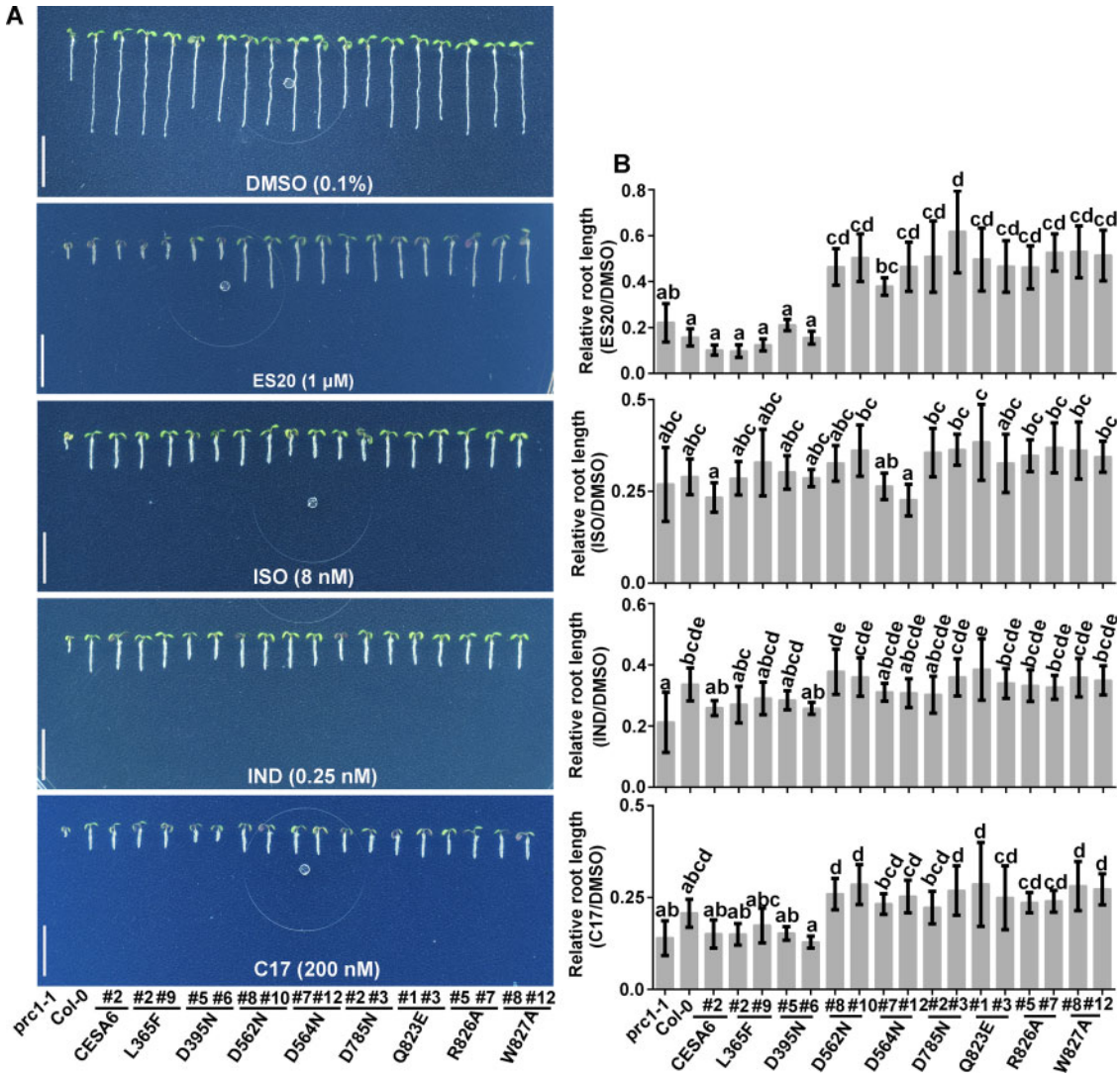

Fig. 4 Plants expressing CESA6 carrying mutations at the predicted binding sites are sensitive to isoxaben, indaziflam and C17. (A) Representative 5-day-old seedlings of *prc1-1/cesa6* complemented with wild-type *CESA6* or mutated *CESA6* carrying predicted mutations at the modeled catalytic site. The plants were grown on $^1/_2$ MS medium supplemented with DMSO (0.1%), ES20 (1 μM), isoxaben (8 nM; ISO), indaziflam (0.25 nM; IND) or C17 (200 nM). Scale bars: 1 cm. (B) Quantification of the relative root lengths of the seedlings shown in (A). Different letters indicate a statistically significant difference ($P < 0.05$), as determined using a one-way ANOVA followed by Tukey's multiple comparison test. The data represent the mean ± SD. $N = 12$.

reduced sensitivity to ES20 are located in the central cytoplasmic domain. We next tested how the isoxaben-insensitive mutants respond to ES20. We grew *ixr1-1*, *ixr1-2* and *ixr2-1* on growth medium supplemented with DMSO (0.1%), isoxaben (10 nM), or ES20 (1 μM) for 5 d. Although the *ixr* mutants displayed reduced sensitivity to isoxaben, as previously reported, they showed the same sensitivity to ES20 as the wild-type plants (**Fig. 5**). These findings further indicate that ES20 and isoxaben target different sites in CESAs.

ES20 has a synergistic inhibitory effect on plant growth with other CBIs

Since ES20 has a different mode of action than isoxaben, indaziflam and C17, we next explored whether ES20 has synergistic effects with these CBIs in inhibiting plant growth. We first tested a series of concentrations of ES20, isoxaben, indaziflam and C17 to determine the maximum concentration for each that does not inhibit the root growth of Col-0 seedlings. As shown in **Fig. 6** and **Supplementary Fig. S3**, 250 nM ES20, 4 nM isoxaben, 0.06 nM indaziflam or 40 nM C17 alone did not significantly inhibit wild-type root growth. Using combined treatments, we found that 250 nM ES20 together with 4 nM isoxaben, 0.06 nM indaziflam or 40 nM C17 significantly inhibited root growth compared with the DMSO control treatment or the individual drug treatments (**Fig. 6**, **Supplementary Fig. S3**). It is possible that our observed more significant inhibitory effects by two inhibitors together are simply an additive effect of two cellulose synthesis inhibitors with different target sites that have led to a more severe effect on root growth in general. However, taken together with our genetic data that some mutants that are resistant to ES20 are sensitive to other inhibitors, these data corroborate a synergistic effect of the ES20 with

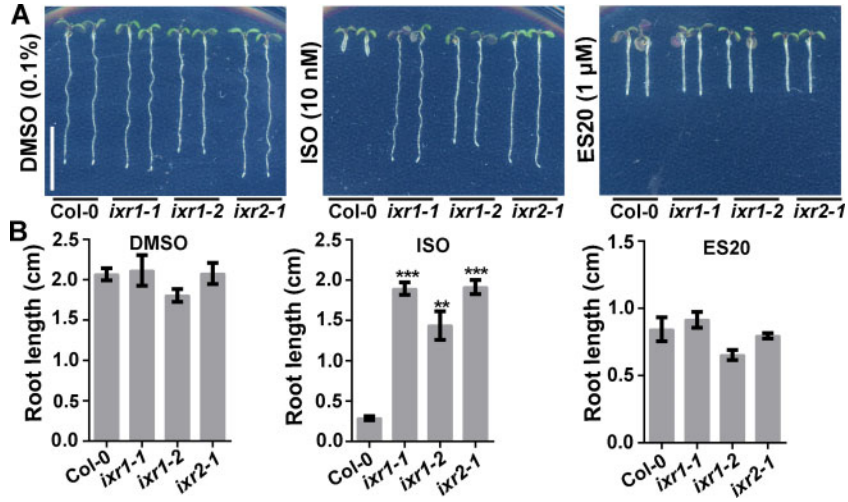

Fig. 5 The isoxaben-resistant mutants are sensitive to ES20. (A) Representative 5-day-old seedlings of Col-0 and the three isoxaben-resistant mutants (*ixr1-1*, *ixr1-2* and *ixr2-1*) grown on $^1/_2$ MS growth medium supplemented with DMSO (0.1%), isoxaben (10 nM; ISO) or ES20 (1 μM). Scale bar: 1 cm. (B) Quantification of the root lengths of the seedlings shown in (A). $^{**}P < 0.01$, $^{***}P < 0.001$ (two-tailed Student's *t*-test) in comparison with Col-0. The data represent the mean ± SD. $N = 9$.

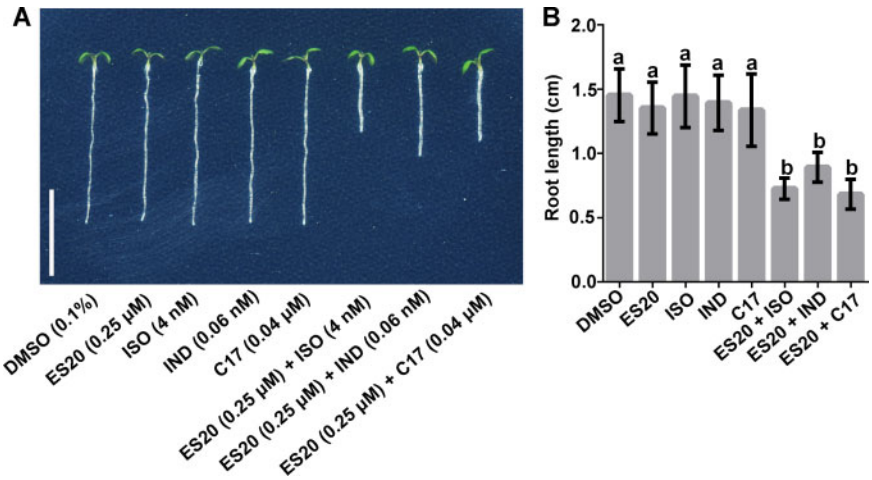

Fig. 6 ES20 has a synergistic inhibitory effect on root growth when combined with isoxaben, indaziflam or C17. (A) Representative 5-day-old Col-0 seedlings grown on $^1/_2$ MS medium supplemented with DMSO (0.1%), ES20 (0.25 μM), isoxaben (4 nM; ISO), indaziflam (0.06 nM; IND), C17 (0.04 μM) and a mixture of ES20 (0.25 μM) and one of the three other inhibitors. Scale bar: 1 cm. (B) Quantification of the root lengths of the seedlings shown in (A). Different letters indicate a statistically significant difference ($P < 0.05$), as determined using a one-way ANOVA followed by Tukey's multiple comparison tests. The data represent the mean ± SD. $N = 15$.

other tested cellulose synthesis inhibitors. These synergistic effects of ES20 with other CBIs in inhibiting root growth further support the idea that ES20 has a different mode of action than isoxaben, indaziflam and C17.

Single amino acid change in CESA6 enables plants to tolerate ES20 without affecting their growth

Among our previously identified ES20-resistant mutants, *es20r1* (CESA6^{E929K}) did not have significantly reduced root growth and displayed the least amount of growth inhibition when treated with ES20 (**Fig. 3**) (Huang et al. 2020). This normal growth pattern and strong tolerance of ES20 indicate that editing *CESA6* is a promising approach for creating ES20-resistant plants. To test this, we introduced a single-nucleotide mutation in the *YFP-CESA6* genomic construct to create the *YFP-CESA6*^{E929K} construct. We then transformed the *YFP-CESA6* and *YFP-CESA6*^{E929K} constructs into the *cesa6* null mutant *prc1-1*, which produces shorter roots under control conditions. We then screened for and obtained independent homozygous single insertion transgenic lines for *YFP-CESA6* and *YFP-CESA6*^{E929K}. We found that the expression of *YFP-CESA6* could rescue the growth defect of *prc1-1* (**Fig. 7A, B**). The *YFP-CESA6* transgenic plants showed the same sensitivity to ES20 as the wild-type plants when grown on a growth medium supplemented with ES20. By contrast, *YFP-CESA6*^{E929K} not only rescued the growth defect of *prc1-1*, but the transgenic plants were also tolerant of ES20, showing normal root growth on media supplemented with ES20. We also grew the transgenic plants on normal growth media and treated them with ES20 overnight. We found that the *YFP-CESA6;prc1-1* plants had

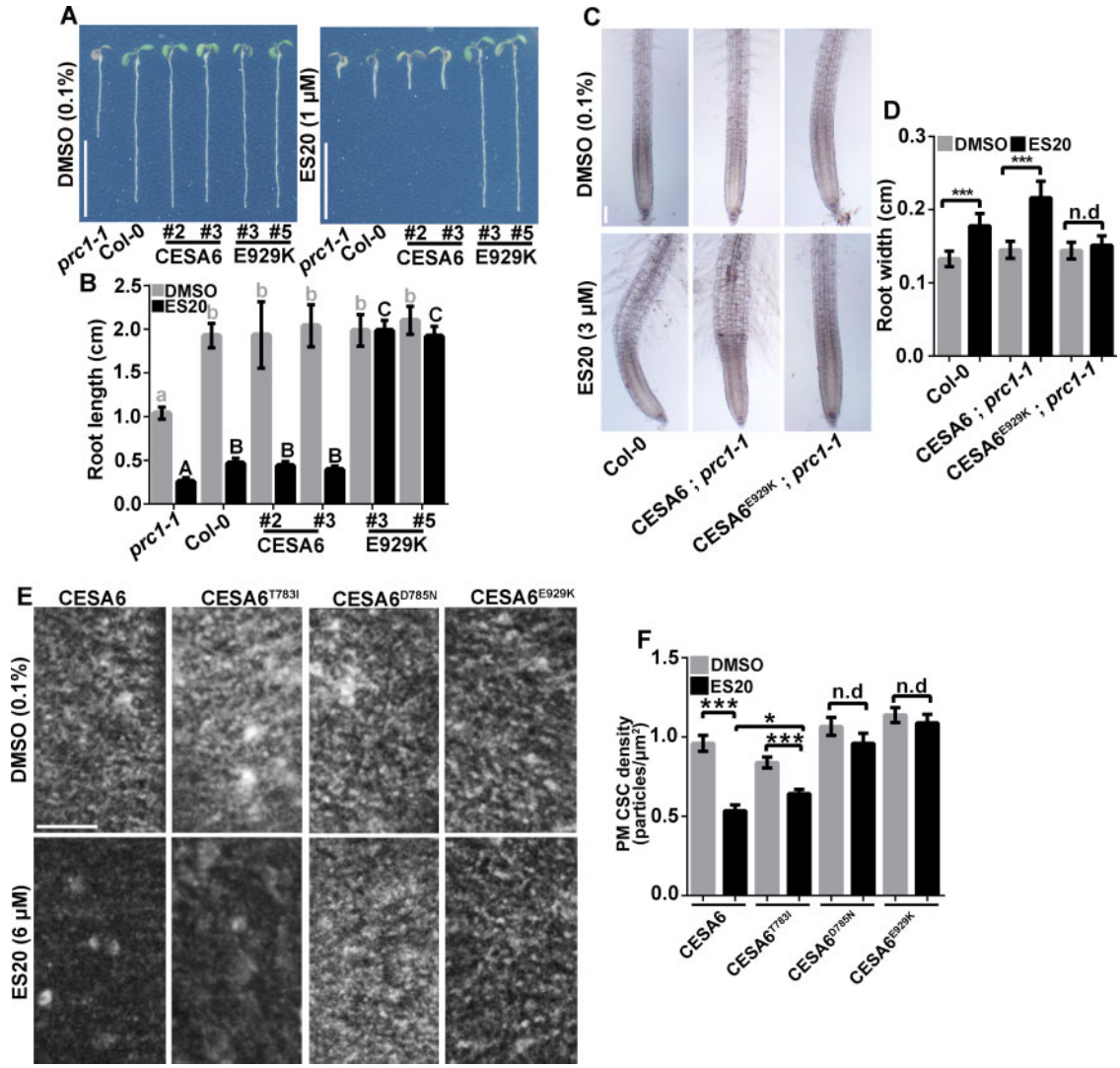

Fig. 7 The *CESA6* point mutation E929K abolishes the inhibitory effect of ES20 on root growth and on the depletion of CSC at the PM. (A) Representative 5-day-old seedlings of *prc1-1*, Col-0 and *prc1-1* complemented with wild-type or mutated *CESA6*. The seedlings were grown on $^1/_2$ MS medium supplemented with DMSO (0.1%) or ES20 (1 μM). Scale bars: 1 cm. (B) Quantification of the root lengths of the seedlings shown in (A). Different letters indicate a statistically significant difference ($P < 0.05$), as determined using a one-way ANOVA followed by Tukey's multiple comparison tests. Lower- and upper- case letters represent the statistical analysis of plants grown on media containing DMSO and ES20, respectively. The data represent the mean ± SD. $N = 10$. (C, D) The *CESA6* point mutation E929K abolishes a swollen root phenotype caused by the ES20 treatment. (C) Representative root images of 5-day-old Col-0 and transgenic plants expressing wild-type or mutated *CESA6* in the *prc1-1* background. The plants were treated with liquid $^1/_2$ MS supplemented with DMSO (0.1%) or ES20 (3 μM) for 20 h. Scale bar: 100 μm. (D) Quantification of the root widths of the seedlings shown in (C). $^{***}P < 0.001$ (two-tailed Student's *t*-test), in comparison with the DMSO treatment, while n.d. indicates no significant difference. The data represent the mean ± SD. $N = 15$. (E, F) The E929K mutation causes a reduced sensitivity to the effect of ES20 treatment on CSC localization. (E) Representative images of PM-localized YFP-CESA6, YFP-CESA6^{T783I,} YFP-CESA6^{D785N} and YFP-CESA6^{E929K} after a 30-min ES20 treatment. Scale bar: 5 μm. (F) Quantification of the density of PM-localized CSC shown in (E). $^{*}P < 0.05$ and $^{***}P < 0.001$ (two-tailed Student's *t*-test), in comparison with the DMSO treatment, while n.d. indicates no significant difference. The data represent the mean ± SE. $N = 24$.

swollen root tips with significantly greater diameters following the ES20 treatment, while the *YFP-CESA6*^{E929K}*;prc1-1* root tips were not swollen under the same ES20 treatment (**Fig. 7C, D**). These growth assays indicate that the *CESA6*^{E929K} mutation enables plants to tolerate ES20.

ES20 targets CESA6 and a short-term ES20 treatment reduces the CSC localization at the PM (Huang et al. 2020). Since YFP-CESA6^{E929K} was sufficient to cause plants to tolerate ES20 and not show ES20-induced growth inhibition and cell swelling, we next investigated whether this ES20 resistance occurs at the subcellular level. We performed a short-term ES20 treatment on the *YFP-CESA6;prc1-1* and *YFP-CESA6*^{E929K}*; prc1-1* plants and examined their CSC localization. Consistent with our previous report (Huang et al. 2020), the *YFP-CESA6; prc1-1* seedlings treated with 6 μM ES20 for 30 min had a significantly reduced CSC density at the PM compared with those subjected to the DMSO control treatment (**Fig. 7E, F**). *YFP-CESA6*^{T783I}*;prc1-1* seedlings treated with 6 μM ES20 for 30 min

also have reduced CSC density at the PM, although the level of reduction upon ES20 treatment is slightly lower than that of *YFP-CESA6;prc1-1* (Fig. 7E, F). By contrast, 30 min of the 6 μM ES20 treatment did not significantly affect the CSC density at the PM in the *YFP-CESA6*^{D785N}*;prc1-1* and *YFP-CESA6*^{E929K}*;prc1-1* seedlings. Thus, a single amino acid change in CESA6 is sufficient to allow plants to tolerate ES20 in terms of plant growth and CSC trafficking at the cellular level and different mutations contribute differently to ES20 sensitivity in growth and in CSC trafficking.

Our previously identified *cesa6* alleles with reduced sensitivity to ES20 provide guidance for generating mutations in other plant species to confer reduced sensitivity to ES20 using genetic engineering. To test whether the reduced ES20 sensitivity trait is dominant or recessive, we transformed three *YFP-CESA6* genomic constructs carrying missense mutations (*YFP-CESA6*^{E929K}, *YFP-CESA6*^{T783I} and *YFP-CESA6*^{D396N}) driven by the native *CESA6* promoter into the Arabidopsis wild-type Col-0 using Agrobacterium-mediated transformation. We grew the transgenic plants expressing *YFP-CESA6*^{E929K}, *YFP-CESA6*^{T783I} and *YFP-CESA6*^{D396N} on growth media supplemented with DMSO (0.1%) or ES20 (1 μM). These transgenic plants did not display obvious growth defects when grown on the DMSO control medium but had longer roots than the non-mutated *YFP-CESA6* plants when grown on growth media supplemented with ES20 (Fig. 8). We also noticed that the plants expressing the mutated *CESA6* constructs in the Col-0 background had a lower level of ES20 resistance than the EMS-generated mutants (Figs. 3, 8), indicating that the reduced sensitivity to ES20 caused by the *cesa6* mutations was semi-dominant.

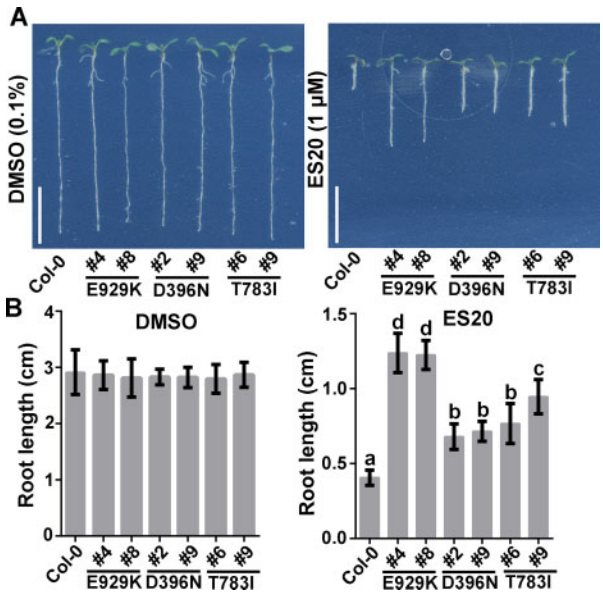

Fig. 8 ES20 tolerance caused by the *cesa6* mutations is a semi-dominant trait. (A) Representative 5-day-old seedlings of Col-0 and the transgenic lines expressing three different mutated *CESA6* constructs (*CESA6*^{E929K}, *CESA6*^{D396N} and *CESA6*^{T783I}) in Col-0. The plants were grown on $^1/_2$ MS medium supplemented with DMSO (0.1%) and ES20 (1 μM). Scale bars: 1 cm. (B) Quantification of the root lengths of the seedlings shown in (A). Different letters indicate a statistically significant difference ($P < 0.05$), as determined using a one-way ANOVA followed by Tukey's multiple comparison tests. The data represent the mean ± SD. $N = 10$.

Generation of a plant with dual resistance to ES20 and isoxaben

Repetitive applications of a single herbicide over long periods of time can be problematic because the selection pressure encourages herbicide-tolerant weeds to grow and herbicide-resistant weeds to emerge through natural mutations (Heap 2014). ES20 and isoxaben seem to target CESAs at different binding sites; therefore, the joint application of ES20 and isoxaben is expected to reduce the likelihood of an herbicide-tolerant weed developing. Establishing a strategy to create crop plants that are resistant to both ES20 and isoxaben is expected to be important for the use of these herbicides in the control of weeds in agricultural production.

We attempted to combine the ES20- and isoxaben-resistant traits by crossing the ES20-resistant mutant *es20r1* (CESA6^{E929K}) with the isoxaben-resistant mutant *ixr1-1* (CESA3^{G998D}). We obtained the homozygous *es20r1;ixr1-1* F_3 generation and tested their growth phenotype on media supplemented with DMSO (0.1%) as the solvent control, ES20 (1 μM), isoxaben (12 nM) or both ES20 (1 μM) and isoxaben (12 nM). As shown in Fig. 9A, B, the *es20r1* and *ixr1-1* single mutant seedlings did not have any obvious root growth defects compared with the wild-type plants when grown on the control growth medium; however, the *es20r1;ixr1-1* double mutant plants had slightly shorter roots (Fig. 9A, B) when grown on media supplemented with DMSO. The single mutant *es20r1* and *ixr1-1* plants had a reduced sensitivity to ES20 or isoxaben, respectively, but the *es20r1;ixr1-1* double mutants could tolerate combined ES20 and isoxaben treatment (Fig. 9A, B).

As the *es20r1;ixr1-1* double mutant seedlings had slightly reduced root growth, we next determined whether they displayed any growth phenotypes at later growth stages. We grew the mutant plants in the soil until the end of their lifecycle and found that the *es20r1* plants have normal-sized rosettes but *ixr1-1* single mutant and *es20r1;ixr1-1* double mutant plants produced smaller rosettes than the wild type (Fig. 9C, D). The height of the 40-day-old soil-grown *es20r1;ixr1-1* double mutant was also shorter than the wild type and the single mutants (Fig. 9E, F). Thus, although the *es20r1;ixr1-1* double mutant can tolerate both ES20 and isoxaben, it does have some trade-offs in terms of growth.

Discussion

CBIs are of significant interest to scientists and agricultural companies (Heim et al. 1990, Brabham et al. 2014, Worden et al. 2015, Hu et al. 2016). These inhibitors allow for the discovery of novel genes or pathways that function in cellulose biosynthesis using sensitivity screens (Scheible et al. 2001, Desprez et al. 2002, Shim et al. 2018), while short-term CBI treatments facilitate the observation of the dynamic behaviors of the CSCs and their regulatory proteins upon the transient

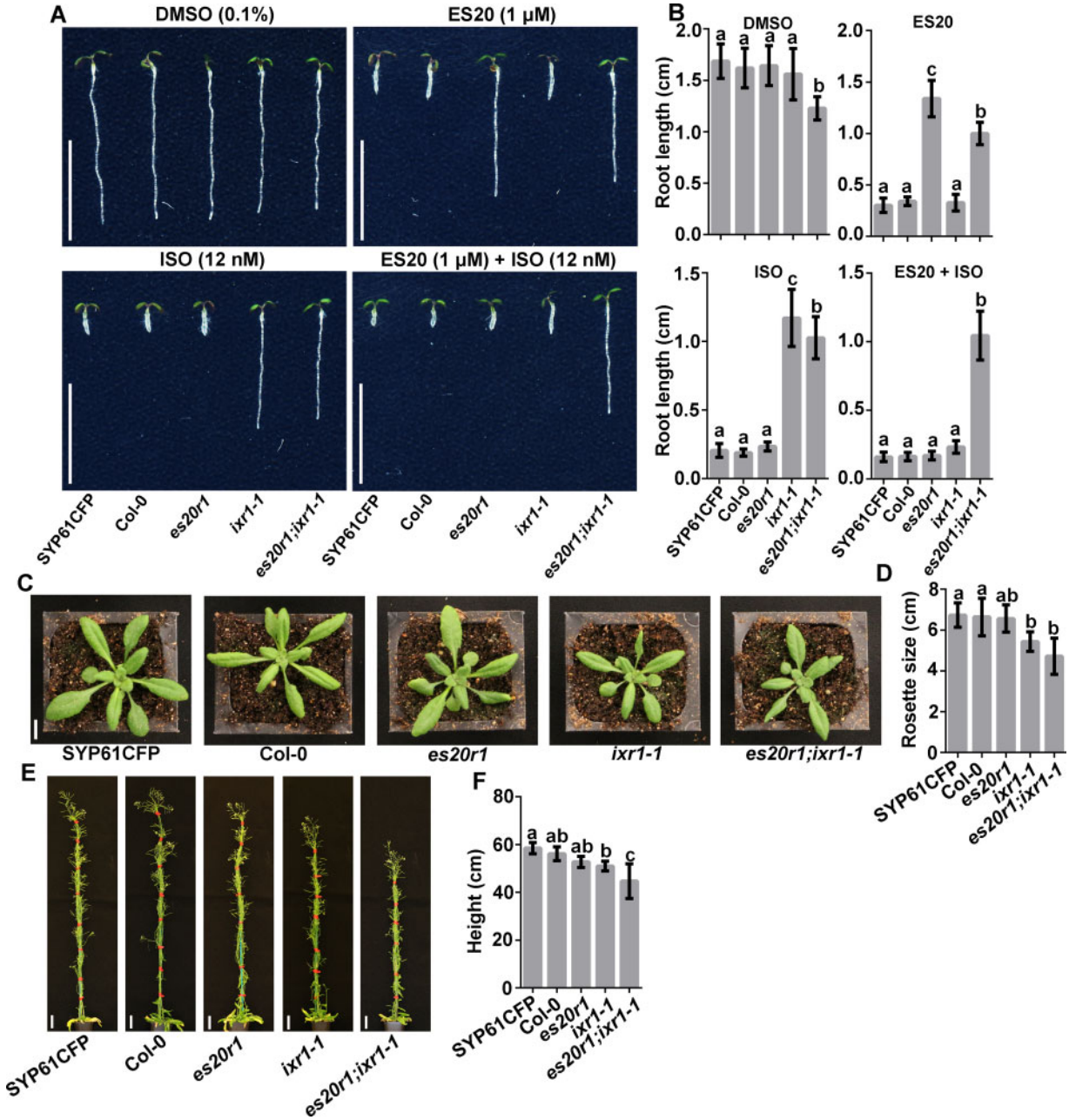

Fig. 9 The *es20r1;ixr1-1* double mutant can tolerate a combined treatment of ES20 and isoxaben. (A, B) The *es20r1;ixr1-1* seedlings exhibit a reduced sensitivity to the combined ES20 and isoxaben treatment. (A) Representative 5-day-old seedlings of SYP61-CFP, Col-0, *es20r1*, *ixr1-1* and *es20r1;ixr1-1*. The plants were grown on $^1/_2$ MS medium supplemented with DMSO (0.1%), ES20 (1 μM), isoxaben (12 nM; ISO) or the combined treatment of ES20 (1 μM) and isoxaben (12 nM). Scale bars: 1 cm. (B) Quantification of the root lengths of the seedlings shown in (A). Different letters indicate a statistically significant difference ($P < 0.05$), as determined using a one-way ANOVA followed by Tukey's multiple comparison tests. The data represent the mean ± SD. $N = 15$. (C) The rosettes of 3-week-old SYP61-CFP, Col-0, *es20r1*, *ixr1-1* and *es20r1;ixr1-1* seedlings grown on soil. Scale bar: 1 cm. (D) Quantification of the size of the rosettes of the 3-week-old soil-grown plants shown in (C). Rosette size was measured as the sum of the lengths of the longest leaf and second longest leaf. The data represent the mean ± SD. $N = 9$. Different letters indicate a statistically significant difference ($P < 0.05$), as determined using a one-way ANOVA followed by Tukey's multiple comparison tests. (E) Representative 40-day-old soil-grown plants of SYP61-CFP, Col-0, *es20r1*, *ixr1-1* and *es20r1;ixr1-1*. Scale bars: 3 cm. (F) Quantification of the height of the soil-grown plants shown in (E). The data represent the mean ± SD. $N = 8$. Different letters indicate a statistically significant difference ($P < 0.05$), as determined using a one-way ANOVA followed by Tukey's multiple comparison tests.

inhibition of cellulose biosynthesis (Montezinos and Delmer 1980, Heim et al. 1989, Scheible et al. 2001, Desprez et al. 2002, Debolt et al. 2007, Brabham et al. 2014, Worden et al. 2015, Hu et al. 2016, Tateno et al. 2016, Tran et al. 2018). Because of the importance of cellulose in plant growth, CBIs are used as herbicides in agricultural production (Schneegurt et al. 1994, Brabham et al. 2014, Hu et al. 2019). The effects of CBIs on plant cellulose biosynthesis and CSC trafficking mean it is reasonable

to assume that some CBIs may target CESAs directly, e.g. isoxaben is likely to target Arabidopsis CESA3 and CESA6 directly (Scheible et al. 2001, Desprez et al. 2002); however, the endogenous cognate proteins for these inhibitors have not been well characterized, which has limited our interpretation of the observations made when using these molecules.

ES20 is a newly identified CBI that shares some characteristics with other known CBIs in terms of cellulose content reduction and the ectopic accumulation of lignin and callose after treatment (Huang et al. 2020). Strong genetic and biochemical evidence suggests that ES20 targets CESA6 at its catalytic site (Huang et al. 2020); however, ES20 has a different mode of action than the other three CBIs tested here, based on two main observations. First, most of the ES20-resistant mutants remain sensitive to the other three CBIs, isoxaben, indaziflam and C17, while all three isoxaben-insensitive mutants were sensitive to ES20. Second, all of the predicted ES20-binding site mutants are sensitive to the other tested CBIs, indicating that the binding site of ES20 differs from the binding sites of the other three CBIs.

Several ES20-resistant mutants show cross-resistance to isoxaben, indaziflam and C17; e.g. *es20r3* (CESA6^{L935E}), *es20r4* (CESA6^{D605N}) and *es20r5* (CESA6^{S360N}) had reduced sensitivity to all four CBIs we tested here (**Fig. 3**). The amino acids L935, D605 and S360 are important for CESA6 function because the plants in which they were mutated have obvious root growth defects (**Fig. 3**). The reduced sensitivities to the CBIs caused by the mutations in these amino acids indicate that these four tested CBIs may share some common features in affecting cellulose biosynthesis, although their exact target sites are different. It is possible that these amino acids are close to the target sites for isoxaben, indaziflam and C17. This will remain an open question because the direct interaction between the CESAs and isoxaben, indaziflam and C17 requires further characterization. This future research will be especially interesting for indaziflam, which seems to act differently than the other CBIs at the cellular level; indaziflam increased the CSC density at the PM, but ES20, isoxaben and C17 decreased the CSC density at the PM (Paredez et al. 2006, Brabham et al. 2014, Hu et al. 2016, Huang et al. 2020). It will be very interesting to investigate why the same mutations can lead to resistance to various CBIs despite their differing effects on CSC subcellular localization.

Weeds compete with crops for the limited resources of nutrition, space, light and water and are thus undesirable in agricultural production. In extreme cases, uncontrolled weeds may cause crop yield losses of over 80% (Heap 2014). Based on their modes of action, herbicides can be further divided into different functional groups, such as photosynthesis inhibitors, acetolactate synthase inhibitors and CBIs (Gianessi 2013). Naturally occurring herbicide-tolerant and herbicide-resistant weeds have become problematic after the repeated usage of a single herbicide due to selection (Delye et al. 2013, Heap 2014). According to the international survey of herbicide-resistant weeds (**http://www.weedscience.org**), 262 weed species (152 dicots and 110 monocots) have been reported to have evolved herbicide resistance to 23 of the 26 known herbicide sites of action, and to 167 different herbicides. A good example is 2,4-D, the well-known synthetic auxin that was commercialized in the 1940s. This herbicide is one of the oldest and most widely used in the control of broad-leaf weeds and woody plants for a variety of small grain, fruit and vegetable crops (Peterson et al. 2016). After over 70 years of applications, >40 weed species have been reported to show resistance to 2,4-D, according to the international survey of herbicide-resistant weeds (**http://www.weedscience.org**). Thus, the identification of novel herbicides is quite urgent to enhance crop production to feed the ever-increasing global population.

CBIs provide valuable resources for commercial herbicide development. CBIs are a class of herbicides with one of the lowest occurrences of weed resistance (Heap 2014). Interestingly, the mutations of different CESAs, especially the primary cell wall-related CESAs 1, 3 and 6, have been found to reduce plant sensitivity to CBIs (Scheible et al. 2001, Desprez et al. 2002, Tateno et al. 2016, Hu et al. 2018). The CBIs and the reduced-sensitivity mutants are therefore valuable resources for the development of novel herbicides and for the breeding of herbicide-resistant crops, which can be accomplished using gene-editing technologies (Hu et al. 2019).

We characterized the inhibitory effect of ES20 on different plant species and found that it is a broad-spectrum plant growth inhibitor with a higher efficiency in dicotyledonous rather than monocotyledonous plants. ES20 has a synergistic inhibitory effect on plant growth when used in combination with other CBIs (**Fig. 6**), which implies that these compounds could be jointly used as herbicides to increase the weed control efficiency and to reduce the development of weed resistance. ES20 can inhibit plant growth in soil, although a relatively high dosage is needed (**Fig. 1Q**). A future optimization of compound's structure will facilitate the development of ES20 into a commercial herbicide with a higher efficiency. Among the 15 identified mutants with a reduced sensitivity to ES20, *CESA6*^{E929K} was the most efficient in tolerating its inhibitory effect. At the cellular level, PM-localized CESA6^{E929K} is not affected by ES20 treatment. This ES20 resistance resulting from a single amino acid change in CESA6 indicates that it could be possible to create ES20- resistant crop species using gene-editing technology. CRISPR-mediated gene editing has been used to generate C17- resistant plants (Hu et al. 2019), and it could also be possible to create ES20- resistant plants using this technology. We also revealed that it is possible to create plants with a dual resistance to ES20 and isoxaben, as was shown for the *es20r1; ixr1-1* double mutant (**Fig. 9**). This double mutant did display slightly reduced root growth, smaller rosettes and a shorter height under the control conditions, however, indicating that the spontaneous mutations of *CESA3* and *CESA6* further affected the normal functioning of the CSC. The previously reported double mutant *cesa1*^{aegeus};*cesa3*$^{ixr1\text{-}2}$, which displays dual resistance to quinoxyphen and isoxaben, also showed a far more pronounced dwarf phenotype than either of the single mutants (Harris et al. 2012). By contrast, the recently reported *CESA3*^{S983F};*ixr2-1*(CESA6^{R1064W}) double mutant shows dual resistance to isoxaben and C17 without any obvious growth phenotypes (Hu et al. 2019), indicating that different combinations

of mutated *CESAs* may affect the plant growth differently and that it is possible to obtain dual-resistant *cesa* mutants without a growth penalty. The resistance of the *es20r1;irx1-1* double mutant to both ES20 and isoxaben suggests that it is worth trying to create double amino acid mutations in *CESA6* in an attempt to confer resistance to both ES20 and isoxaben without affecting growth.

Taking our results together, we showed that ES20 has a different mode of action to isoxaben, indaziflam or C17. ES20 has a synergistic effect with these other CBIs in inhibiting plant growth. ES20 could be used as a potential spray herbicide, and it is possible to create plants that can tolerate both ES20 and isoxaben using gene-editing technologies.

Materials and Methods

Plant materials and growth conditions

To test the effect of ES20 on different plant species, *A. thaliana* Col-0, tomato Micro-tom, soybean Williams 82, maize B73, rice Nipponbare, perennial ryegrass Bright star and Kentucky bluegrass Brilliant were used. Dandelion seeds were collected from a wild population in West Lafayette, Indiana, USA. The seeds of Arabidopsis, dandelion, tomato, soybean, maize and rice were sterilized and sown on $\frac{1}{2}$ MS medium containing 0.8% agar (pH 5.8) and different concentrations of ES20. The plants were grown vertically under continuous light (130 μmol m^{-2} s^{-1} intensity) at 22°C. The Kentucky bluegrass and perennial ryegrass seeds were directly grown on filter paper soaked in sterile water supplemented with DMSO (0.1%) or ES20 (50 μM) at 22°C.

Different CBI treatments and ES20 structure–activity relationship analysis

To test the sensitivity of the *es20r* mutants and the CESA binding site mutants to the different CBIs, the sterilized Arabidopsis seeds were grown vertically on $\frac{1}{2}$ MS medium supplemented with the indicated concentrations of the CBIs. An equal volume of DMSO was used as a control. After 5 d of growth, the plates were scanned using an Epson Perfection V550 scanner (Epson, 3 Chome-3-5 Owa, Suwa, Nagano 392-0001, Japan) and the resulted images were used for root length quantification using ImageJ (**https://imagej.nih.gov/ij/index.html, October 21, 2020, date last accessed**). Representative seedlings grown on different CBIs were selected and placed on an agar plate. The plate was then scanned using an Epson Perfection V550 scanner to obtain images for representative seedlings. To test the structure–activity relationship of ES20, 11 ES20 analogs were ordered from Vitascreen (Vitascreen, University of Illinois Urbana-Champaign Research Park, 2001 South First Street, Suite 201, Champaign, IL, 61820, USA). Sterilized Arabidopsis Col-0 seeds were grown on $\frac{1}{2}$ MS medium supplemented with 1 μM of ES20 or the different analogs. An equal volume of DMSO was used as a control. After 5 d of vertical growth, the plates were scanned using an Epson Perfection V550 scanner and the resulted images were used for root length quantification using ImageJ. Representative seedlings grown on different analogs were selected and placed on an agar plate. The plate was then scanned using an Epson Perfection V550 scanner to obtain images for representative seedlings.

Generation of transgenic Arabidopsis plants

The *YFP-CESA6*^{E929K} construct was created as described previously (Huang et al. 2020). Briefly, the genomic construct containing the *CESA6* gene and its endogenous promoter was cloned into the modified binary vector pH7WGR2, from which the *35S* promoter and RFP-tag had been removed. The *YFP* tag was inserted into the N-terminal region of the *CESA6* start codon. The mutation *E929K* was introduced using site-directed mutagenesis. The verified plasmids were transformed into Col-0 or the *CESA6* null mutant *prc1-1* (CS297) using *Agrobacterium tumefaciens*-mediated floral dipping (Clough and Bent 1998). The *prc1-1* seeds were obtained from the Arabidopsis Biological Resource Center.

Live-cell imaging with spinning-disk confocal microscopy

Spinning-disk confocal microscopy (SDCM) was used to examine the localization of the CSCs at the PM. The seedlings of *YFP-CESA6;prc1-1*, *YFP-CESA6*^{E929K}*;prc1-1*, *YFP-CESA6*^{T783I}*;prc1-1* and *YFP-CESA6*^{D785N}*;prc1-1* grown on $\frac{1}{2}$ MS medium for 5 d in a vertical orientation were treated with DMSO or 6 μM ES20 for 30 min. Two thin strips of double-sided tape were placed onto glass slides about 2 cm apart. A 100-μl aliquot of $\frac{1}{2}$ MS liquid growth medium containing DMSO (0.1%) or 6 μM ES20 was applied to the glass slides, into which the seedlings were carefully mounted using tweezers. A 22-mm × 40-mm cover glass was placed on top of the double-sided tape for imaging. Images were taken off the 2nd or 3rd epidermal cells below the first obvious initiated root hair in the root elongation region using a CSU-X1-A1 scanner unit (Yokogawa Electric, 2-9-32 Nakacho, Musashino, Tokyo, Tokyo 180-8750, Japan) mounted on an Olympus IX-83 microscope (Olympus, 2-3-1 Nishi-Shinjuku, Shinjuku-ku, Tokyo, 163-0914, Japan) equipped with a 100× 1.45-numerical aperture UPlanSApo oil objective (Olympus, 2-3-2 Nishi-Shinjuku, Shinjuku-ku, Tokyo, 163-0914, Japan) and an Andor iXon Ultra 897BV EMCCD camera (Oxford Instruments, Tubney Wood, Sandleigh, Abingdon-on-Thames, UK). YFP fluorescence was excited with a 515-nm laser and the emissions were collected using a 542/27-nm filter.

PM-localized CSC density analysis

To examine the effect of ES20 on the PM-localized CSC density, the SDCM images were analyzed using ImageJ. The Freehand selection tool was used to select a region of interest (ROI) avoiding CSCs from the Golgi. The CSC particles from the selected ROIs were detected on 8-bit images using the Find Maxima tool with the same noise threshold for all images. The CSC particle density was calculated by dividing the number of particles by the ROI area.

ES20 spray test on soil-grown plants

Arabidopsis Col-0 seedlings grown on $\frac{1}{2}$ MS growth medium for 5 d were transferred into soil and covered with a transparent plastic lid for 2 d. The plants were then sprayed with 50 ml of sterile water supplemented with DMSO (0.5%) or ES20 (500 μM). The plants were imaged 7 d after spraying.

Supplementary Data

Supplementary data are available at PCP online.

Acknowledgments

We thank Dr. Yiwei Jiang for sharing the seeds of Kentucky bluegrass and perennial ryegrass and Dr. Cankui Zhang for sharing the rice seeds. We thank Dr. Christopher J. Staiger for allowing us to use the spinning-disk confocal microscope to image the CSC localization and Dr. Weiwei Zhang for providing the training on operating the spinning-disk confocal microscope and image analysis.

Funding

Trask Trust Fund (41000604 to C.Z.); Purdue University provost's startup fund (to C.Z.); and National Science Foundation (2025437-MCB to C.Z.).

Authors' Contributions

L.H. performed all the experiments and wrote the manuscript draft. C.Z. conceived the experiments and revised the manuscript. Both authors have read and approved the manuscript.

Disclosures

The authors have no conflicts of interest to declare.

References

Bashline, L., Li, S., Anderson, C.T., Lei, L. and Gu, Y. (2013) The endocytosis of cellulose synthase in Arabidopsis is dependent on mu2, a clathrin-mediated endocytosis adaptin. *Plant Physiol.* 163: 150–160.

Brabham, C., Lei, L., Gu, Y., Stork, J., Barrett, M. and Debolt, S. (2014) Indaziflam herbicidal action: a potent cellulose biosynthesis inhibitor. *Plant Physiol.* 166: 1177–1185.

Bringmann, M., Li, E., Sampathkumar, A., Kocabek, T., Hauser, M.T. and Persson, S. (2012) POM-POM2/cellulose synthase interacting1 is essential for the functional association of cellulose synthase and microtubules in Arabidopsis. *Plant Cell* 24: 163–177.

Brinkmeyer, R.S., Terando, N.H., Waldrep, T.W. and Burow, K.W. (1989) The synthesis and biological-activity of heterocyclic-analogs of the broadleaf herbicide isoxaben. *Am. Chem. Soc.* 197: 56-Agro.

Clough, S.J. and Bent, A.F. (1998) Floral dip: a simplified method for Agrobacterium-mediated transformation of *Arabidopsis thaliana*. *Plant J.* 16: 735–743.

Crowell, E.F., Bischoff, V., Desprez, T., Rolland, A., Stierhof, Y.D., Schumacher, K., et al. (2009) Pausing of Golgi bodies on microtubules regulates secretion of cellulose synthase complexes in Arabidopsis. *Plant Cell* 21: 1141–1154.

Debolt, S., Gutierrez, R., Ehrhardt, D.W., Melo, C.V., Ross, L., Cutler, S.R., et al. (2007) Morlin, an inhibitor of cortical microtubule dynamics and cellulose synthase movement. *Proc. Natl. Acad. Sci. USA* 104: 5854–5859.

Delye, C., Jasieniuk, M. and Le Corre, V. (2013) Deciphering the evolution of herbicide resistance in weeds. *Trends Genet.* 29: 649–658.

Desprez, T., Juraniec, M., Crowell, E.F., Jouy, H., Pochylova, Z., Parcy, F., et al. (2007) Organization of cellulose synthase complexes involved in primary cell wall synthesis in *Arabidopsis thaliana*. *Proc. Natl. Acad. Sci. USA* 104: 15572–15577.

Desprez, T., Vernhettes, S., Fagard, M., Refregier, G., Desnos, T., Aletti, E., et al. (2002) Resistance against herbicide isoxaben and cellulose deficiency caused by distinct mutations in same cellulose synthase isoform CESA6. *Plant Physiol.* 128: 482–490.

Doblin, M.S., Kurek, I., Jacob-Wilk, D. and Delmer, D.P. (2002) Cellulose biosynthesis in plants: from genes to rosettes. *Plant Cell Physiol.* 43: 1407–1420.

Endler, A., Kesten, C., Schneider, R., Zhang, Y., Ivakov, A., Froehlich, A., et al. (2015) A mechanism for sustained cellulose synthesis during salt stress. *Cell* 162: 1353–1364.

Fernandes, A.N., Thomas, L.H., Altaner, C.M., Callow, P., Forsyth, V.T., Apperley, D.C., et al. (2011) Nanostructure of cellulose microfibrils in spruce wood. *Proc. Natl. Acad. Sci. USA* 108: E1195–E1203.

Fujita, M., Himmelspach, R., Ward, J., Whittington, A., Hasenbein, N., Liu, C., et al. (2013) The anisotropy1 D604N mutation in the Arabidopsis cellulose synthase1 catalytic domain reduces cell wall crystallinity and the velocity of cellulose synthase complexes. *Plant Physiol.* 162: 74–85.

Gianessi, L.P. (2013) The increasing importance of herbicides in worldwide crop production. *Pest Manag. Sci.* 69: 1099–1105.

Giddings, T.H., Jr, Brower, D.L. and Staehelin, L.A. (1980) Visualization of particle complexes in the plasma membrane of Micrasterias denticulata associated with the formation of cellulose fibrils in primary and secondary cell walls. *J. Cell Biol.* 84: 327–339.

Gonneau, M., Desprez, T., Guillot, A., Vernhettes, S. and Hofte, H. (2014) Catalytic subunit stoichiometry within the cellulose synthase complex. *Plant Physiol.* 166: 1709–1712.

Gu, Y., Kaplinsky, N., Bringmann, M., Cobb, A., Carroll, A., Sampathkumar, A., et al. (2010) Identification of a cellulose synthase-associated protein required for cellulose biosynthesis. *Proc. Natl. Acad. Sci. USA* 107: 12866–12871.

Gutierrez, R., Lindeboom, J.J., Paredez, A.R., Emons, A.M. and Ehrhardt, D.W. (2009) Arabidopsis cortical microtubules position cellulose synthase delivery to the plasma membrane and interact with cellulose synthase trafficking compartments. *Nat. Cell Biol.* 11: 797–806.

Haigler, C.H. and Brown, R.M.J. (1986) Transport of rosettes from the Golgi apparatus to the plasma membrane in isolated mesophyll cells of Zinnia elegans during differentiation to tracheary elements in suspension culture. *Protoplasma* 134: 111–120.

Harris, D.M., Corbin, K., Wang, T., Gutierrez, R., Bertolo, A.L., Petti, C., et al. (2012) Cellulose microfibril crystallinity is reduced by mutating C-terminal transmembrane region residues CESA1A903V and CESA3T942I of cellulose synthase. *Proc. Natl. Acad. Sci. USA* 109: 4098–4103.

Heap, I. (2014) Global perspective of herbicide-resistant weeds. *Pest Manag. Sci.* 70: 1306–1315.

Heim, D.R., Roberts, J.L., Pike, P.D. and Larrinua, I.M. (1989) Mutation of a locus of *Arabidopsis thaliana* confers resistance to the herbicide isoxaben. *Plant Physiol.* 90: 146–150.

Heim, D.R., Skomp, J.R., Tschabold, E.E. and Larrinua, I.M. (1990) Isoxaben inhibits the synthesis of acid insoluble cell-wall materials in *Arabidopsis thaliana*. *Plant Physiol.* 93: 695–700.

Hill, J.L., Jr, Hammudi, M.B. and Tien, M. (2014) The Arabidopsis cellulose synthase complex: a proposed hexamer of CESA trimers in an equimolar stoichiometry. *Plant Cell* 26: 4834–4842.

Hu, Z., Vanderhaeghen, R., Cools, T., Wang, Y., De Clercq, I., Leroux, O., et al. (2016) Mitochondrial defects confer tolerance against cellulose deficiency. *Plant Cell* 28: 2276–2290.

Hu, Z., Zhang, T., Rombaut, D., Decaestecker, W., Xing, A., D'Haeyer, S., et al. (2019) Genome-editing based engineering of CESA3 dual cellulose-inhibitor resistant plants. *Plant Physiol.* 180: 827–836.

Hu, H., Zhang, R., Tao, Z., Li, X., Li, Y., Huang, J., et al. (2018) Cellulose synthase mutants distinctively affect cell growth and cell wall integrity for plant biomass production in Arabidopsis. *Plant Cell Physiol.* 59: 1144–1157.

Huang, L., Li, X., Zhang, W., Ung, N., Liu, N., Yin, X., et al. (2020) Endosidin20 targets the cellulose synthase catalytic domain to inhibit cellulose biosynthesis. *Plant Cell* 32: 2141–2157.

Huggenberger, F. and Gueguen, F. (1987) Yield response to preemergence control of broad-leaved weeds in winter cereals with isoxaben in France. *Crop Protection* 6: 75–81.

Jamet, P. and Thoisy-Dur, J.-C. (1988) Pesticide mobility in soils—assessment of the movement of isoxaben by soil thin-layer chromatography. *Bull. Environ. Contam. Toxicol.* 41: 135–142.

Jarvis, M.C. (2018) Structure of native cellulose microfibrils, the starting point for nanocellulose manufacture. *Philos. Trans. A Math. Phys. Eng. Sci.* 376:20170045.

Kubicki, J.D., Yang, H., Sawada, D., O'Neill, H., Oehme, D. and Cosgrove, D. (2018) The shape of native plant. *Sci. Rep.* 8: 13983.

Lei, L., Li, S. and Gu, Y. (2012) Cellulose synthase interactive protein 1 (CSI1) mediates the intimate relationship between cellulose microfibrils and cortical microtubules. *Plant Signal. Behav.* 7: 714–718.

Meyerowitz, E.M. (1989) Arabidopsis, a useful weed. *Cell* 56: 263–269.

Montezinos, D. and Delmer, D.P. (1980) Characterization of inhibitors of cellulose synthesis in cotton fibers. *Planta* 148: 305–311.

Mueller, S.C. and Brown, R.M. (1980) Evidence for an intramembrane component associated with a cellulose microfibril-synthesizing complex in higher plants. *J Cell Biol.* 84: 315–326.

Mueller, S.C., Brown, R.M., Jr and Scott, T.K. (1976) Cellulosic microfibrils: nascent stages of synthesis in a higher plant cell. *Science* 194: 949–951.

Newman, R.H., Hill, S.J. and Harris, P.J. (2013) Wide-angle x-ray scattering and solid-state nuclear magnetic resonance data combined to test models for cellulose microfibrils in mung bean cell walls. *Plant Physiol.* 163: 1558–1567.

Nixon, B.T., Mansouri, K., Singh, A., Du, J., Davis, J.K., Lee, J.G., et al. (2016) Comparative structural and computational analysis supports eighteen cellulose synthases in the plant cellulose synthesis complex. *Sci. Rep.* 6: 28696.

Oehme, D.P., Downton, M.T., Doblin, M.S., Wagner, J., Gidley, M.J. and Bacic, A. (2015) Unique aspects of the structure and dynamics of elementary Ibeta cellulose microfibrils revealed by computational simulations. *Plant Physiol.* 168: 3–17.

Paredez, A.R., Somerville, C.R. and Ehrhardt, D.W. (2006) Visualization of cellulose synthase demonstrates functional association with microtubules. *Science* 312: 1491–1495.

Persson, S., Paredez, A., Carroll, A., Palsdottir, H., Doblin, M., Poindexter, P., et al. (2007) Genetic evidence for three unique components in primary cell-wall cellulose synthase complexes in Arabidopsis. *Proc Natl Acad Sci USA* 104: 15566–15571.

Peterson, M.A., Mcmaster, S.A., Riechers, D.E., Skelton, J. and Stahlman, P.W. (2016) 2,4-D past, present, and future: a review. *Weed Technol.* 30: 303–345.

Polko, J.K., Barnes, W.J., Voiniciuc, C., Doctor, S., Steinwand, B., Hill, J.L., et al. (2018) SHOU4 proteins regulate trafficking of cellulose synthase complexes to the plasma membrane. *Curr. Biol.* 28: 3174–3182.e6.

Purushotham, P., Ho, R. and Zimmer, J. (2020) Architecture of a catalytically active homotrimeric plant cellulose synthase complex. *Science* 369: 1089–1094.

Sampathkumar, A., Gutierrez, R., Mcfarlane, H.E., Bringmann, M., Lindeboom, J., Emons, A.M., et al. (2013) Patterning and lifetime of plasma membrane-localized cellulose synthase is dependent on actin organization in Arabidopsis interphase cells. *Plant Physiol.* 162: 675–688.

Scheible, W.R., Eshed, R., Richmond, T., Delmer, D. and Somerville, C. (2001) Modifications of cellulose synthase confer resistance to isoxaben and thiazolidinone herbicides in Arabidopsis Ixr1 mutants. *Proc. Natl. Acad. Sci. USA* 98: 10079–10084.

Schneegurt, M.A., Roberts, J.L., Bjelk, L.A. and Gerwick, B.C. (1994) Postemergence activity of isoxaben. *Weed Technol.* 8: 183–189.

Shim, I., Law, R., Kileeg, Z., Stronghill, P., Northey, J.G.B., Strap, J.L., et al. (2018) Alleles causing resistance to isoxaben and flupoxam highlight the significance of transmembrane domains for CESA protein function. *Front. Plant Sci.* 9: 1152.

Tateno, M., Brabham, C. and Debolt, S. (2016) Cellulose biosynthesis inhibitors—a multifunctional toolbox. *J. Exp. Bot.* 67: 533–542.

Taylor, N.G., Howells, R.M., Huttly, A.K., Vickers, K. and Turner, S.R. (2003) Interactions among three distinct CesA proteins essential for cellulose synthesis. *Proc. Natl. Acad. Sci. USA* 100: 1450–1455.

Tran, M.L., Mccarthy, T.W., Sun, H., Wu, S.Z., Norris, J.H., Bezanilla, M., et al. (2018) Direct observation of the effects of cellulose synthesis inhibitors using live cell imaging of Cellulose Synthase (CESA) in Physcomitrella patens. *Sci. Rep.* 8: 735.

Turner, S. and Kumar, M. (2018) Cellulose synthase complex organization and cellulose microfibril structure. *Philos. Trans. A Math. Phys. Eng. Sci.* 376:20170048.

Wang, T. and Hong, M. (2016) Solid-state NMR investigations of cellulose structure and interactions with matrix polysaccharides in plant primary cell walls. *J. Exp. Bot.* 67: 503–514.

Wang, T., Park, Y.B., Cosgrove, D.J. and Hong, M. (2015) Cellulose-pectin spatial contacts are inherent to never-dried arabidopsis primary cell walls: evidence from solid-state nuclear magnetic resonance. *Plant Physiol.* 168: 871–884.

Worden, N., Wilkop, T.E., Esteve, V.E., Jeannotte, R., Lathe, R., Vernhettes, S., et al. (2015) CESA trafficking inhibitor inhibits cellulose deposition and interferes with the trafficking of cellulose synthase complexes and their associated proteins KORRIGAN1 and POM2/CELLULOSE SYNTHASE INTERACTIVE PROTEIN1. *Plant Physiol.* 167: 381–393.

Xia, Y., Lei, L., Brabham, C., Stork, J., Strickland, J., Ladak, A., et al. (2014) Acetobixan, an inhibitor of cellulose synthesis identified by microbial bioprospecting. *PLoS One* 9: e95245.

Yu, J., Schumann, A.W., Cao, Z., Sharpe, S.M. and Boyd, N.S. (2019) Weed detection in perennial ryegrass with deep learning convolutional neural network. *Front. Plant Sci.* 10: 1422.

Zhang, W., Cai, C. and Staiger, C.J. (2019) Myosins XI are involved in exocytosis of cellulose synthase complexes. *Plant Physiol.* 179: 1537–1555.

Zhang, Y., Nikolovski, N., Sorieul, M., Vellosillo, T., Mcfarlane, H.E., Dupree, R., et al. (2016) Golgi-localized STELLO proteins regulate the assembly and trafficking of cellulose synthase complexes in Arabidopsis. *Nat. Commun.* 7: 11656.

Zhu, X., Li, S., Pan, S., Xin, X. and Gu, Y. (2018) CSI1, PATROL1, and exocyst complex cooperate in delivery of cellulose synthase complexes to the plasma membrane. *Proc. Natl. Acad. Sci. USA* 115: E3578–E3587.